A PEEC-Based Concise Broadband Physical Circuit Modeling Method With Parameter Extraction for PCB Inductive Components

Junping He, *Member, IEEE*, Sili Tao, and Huazhao Wu

***Abstract*—Broadband circuit models and their parameters of passive components are an important part of the functional design and electromagnetic compatibility analysis of power electronic devices. In this article, we propose a novel concise physical lumped-parameter extraction method for the construction of effective broadband circuit models for printed circuit board inductive components. The method is based on PEEC theory and generalized eigenvalue theory. The frequency domain port impedance characteristics are kept as equal as possible during circuit model transformation processes. A partial equivalent element circuit (PEEC) model of a three-dimensional PCB inductive component with a large number of nodes is first of all introduced. This includes conductors and PCB dielectrics. Then, its port impedance matrix formula is deduced. After this, the polynomial form of the port impedance matrix and the circuit model order reduction method are presented in detail. We report on the construction of two typical coreless PCB planar components, a spiral planar inductor and a coreless planar transformer, whose broadband physical circuit models and parameters were extracted using the proposed method. The results of tests with these two planar components confirmed the validity of their models for a frequency range of up to 500 MHz.**

***Index Terms*—Circuit parameter extraction, coreless inductive component, generalized eigenvalue theory, partial equivalent element circuit (PEEC).**

I. Introduction

OBTAINING a higher operating frequency has been a strong driving force for the electronics industry for some time and looks set to remain so for the foreseeable future [1]. The switching frequency of a very high frequency power converter has now reached tens of MHz with up-to-date gallium nitride devices, which are much faster than several hundred kHz metallic oxide semiconductor field effect transistor (MOSFET) devices [2]. Modern switched-mode-power-supplies (SMPS) demand a wider frequency band and a more accurate performance from their passive components or interconnections, e.g., inductors, transformers and capacitors, to complete their intended function. Additionally, the electromagnetic compatibility (EMC) design of an SMPS needs precise parasitic circuit parameters among its components and metal structures to help analyze or predict its electromagnetic noise emissions [3], [4]. Thus, both the power electronics industry and academia have an urgent need for an effective way of modeling broadband circuits and their passive components and interconnections [5], [6]. However, predicting and extracting the high frequency parameters of passive devices in advance is quite challenging because of their complex structure and medium.

In view of their importance as an energy storage element, wideband circuit models of inductive components have long been a subject of interest for research. This has included circuit dynamic simulation, electromagnetic analysis, and loss calculation [6]–[10]. Both behavioral modeling methods and analytic modeling methods are often turned to for this. For the former, black box or gray box methods are commonly used in engineering [7], [8]. However, they are heavily dependent on measurements and can't realize predictions in advance. The physical meaning of their circuit models is often unclear too. For analytic modeling, transmission line theory is often used for regular structural components [9], [10]. However, this method has difficulty with irregular device structures and its effective bandwidth is usually below the first resonance point.

In recent years, a method for establishing the circuit model of inductive devices from a 3-D physical structure by using electromagnetic field theory has been developing rapidly [11], [12]. This method has a strong theoretical grounding and significant application value. Thus, it has begun to be used in electromagnetic commercial software for industry [13], [14]. Examples here include the finite-element analysis (FEA) based Ansoft Q3D software and the Fasthenry tool that uses a partial equivalent element circuit (PEEC) approach. In comparison to FE, PEEC theory is better able to transfer the electromagnetic field domain directly into a circuit domain and its equivalent circuit represents the real physical parameters of the actual geometry [15]. PEEC is therefore widely used in integrated chip (IC) design and inductive or capacitive component modeling. Kovačević *et al.* [11] have used the PEEC method to extract the coupling parameters from an electromagnetic interference (EMI) filter and analyze their influence. Enohnyaket and Ekm have also set up the circuit model of an air core inductor using PEEC [16]. However, shortcomings remain regarding the modeling of 3-D electromagnetic

Manuscript received April 30, 2019; revised August 23, 2019 and December 3, 2019; accepted March 12, 2020. Date of publication March 18, 2020; date of current version June 23, 2020. This work was supported in part by the National Natural Science Foundation of China under Grant 51677035 and in part by the Shenzhen City Fundamental Research Plan under Grant JCYJ20160531190745967. Recommended for publication by Associate Editor L.Wang. *(Corresponding author: Junping He.)*

The authors are with the Harbin Institute of Technology, Shenzhen 518055, China (e-mail: hejunping@hit.edu.cn; 1148861220@qq.com; 791710477@qq.com).

Color versions of one or more of the figures in this article are available online at http://ieeexplore.ieee.org.

Digital Object Identifier 10.1109/TPEL.2020.2981952

structures. One issue is the large number of cells that are often used to obtain wider bandwidth and better accuracy. This makes computation of the circuit model very time-consuming and resource hungry. To make matters worse, it is hard for a designer to obtain direct physical insights from so many circuit components. To reduce the complexity of the model, model order reduction (MOR) techniques have been developed [17], [18]. However, many MOR methods, such as the Krylov subspace method and the piecewise linear method, are only simplified through mathematical calculations, so the simplified model's parameters often lose their physical meaning. Thus, a reduced order circuit model that keeps both its physical meaning and a wide frequency band performance is urgently required. Bondarenko *et al.* [19] have tried to develop a simple physics-based circuit macromodel with PEEC by extracting inductance and capacitance parameters. Unfortunately, this method can only guarantee characteristics around the first resonance point. Dou and Wu [20] proposed a general and physically meaningful method that absorbs insignificant PEEC nodes, which keeps passivity and fidelity, and is fit for time or frequency domain simulation. However, some EMC prediction applications need higher MOR capabilities.

In view of the earlier situation, this paper presents a novel concise modeling method for coreless inductive components that can obtain simplified broadband circuits from a large-scale PEEC model, whilst retaining their physical meaning. This method uses generalized eigenvalue theory, as proposed by Filex Traub *et al.* [21], [22]. Filex Traub found that a generalized eigenvalue relationship exists among the resonant modes and the admittance matrix of a lossless physical system and he extracted the corresponding *L* and *C* parameters based on finite element physical model. However, the finite-element numerical modeling and analysis is very professional tool, and it would be more convenient for electrical engineers to extract lumped parameters based on the circuit modeling. Therefore, the article extracts the concise lumped circuit parameters through the 3-D PEEC model. The impedance parameters of the concise PEEC circuit model can clearly indicate how they relate to actual geometry and the model's port impedance characteristics are maintained in the broadband range.

The article is organized as follows. In Section II, PEEC formulations of conductor and dielectric materials are introduced. In Section III, we present and explain in detail a wide frequency band lumped circuit parameter extraction method. In Section IV, we describe the construction of two planar inductive component models, a spiral planar PCB inductor and a planar PCB transformer, and extract their circuit parameters using the proposed method. Simulations and measurements were conducted to validate the feasibility of the model and its error characteristics are analyzed and discussed at the end.

II. PEEC Formulation for Planar PCB Components

PEEC is a circuit-oriented electromagnetic approach that converts an integral equations-based solution of Maxwell's equations into appropriate equivalent circuits. These equivalent circuits establish the relationship between circuit parameters

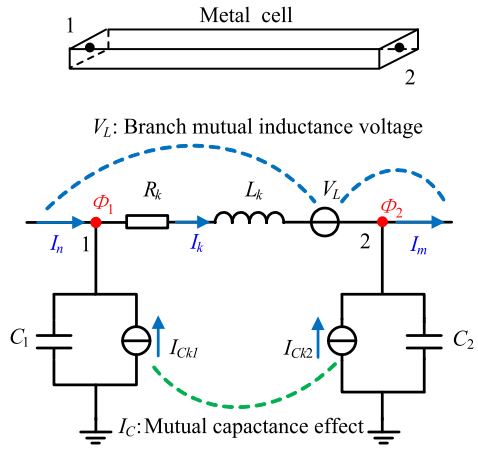

Fig. 1. Basic PEEC model of a metal cell.

(e.g., partial inductance and partial capacitance) and geometries. They are also easy to solve and analyze in both time and frequency domains by using modern-day circuit simulation tools. Generally, the PEEC approach to creating electromagnetic models involves structure meshing, equivalent circuit parameter calculation and matrix formulation.

As the size of the objects of this study are much smaller than the length of the highest frequency electromagnetic wave concerned, a quasi-static PEEC method is sufficiently accurate to be able set up and analyze a model [16]. The basic formulation of a quasi-static PEEC is presented below. More details can be found in [15].

A. PEEC Elements for PCBs: Conductors and Dielectrics

To model the conductors in a PCB inductive component, two meshing schemes are often used: a volume-cell mesh for the current distribution; and a surface-cell mesh for the charge distribution. A typical PEEC model of a metal media cell is shown in Fig. 1. Resistor R_k represents the loss of conductivity between nodes 1 and 2; L_k represents the inductance of this conductor; C_1 and C_2 represent the self-capacitance of nodes 1 and 2, respectively; V_L is a current-controlled voltage source, which represents the mutual inductance between different inductive meshes; I_{Ck1}, and I_{Ck2} are current-controlled current sources, which represent the mutual capacitance between capacitive meshes.

For the dielectrics of PCB inductive components, volume-cell and surface-cell meshes are similarly used to model the distribution of current and charge. A typical PEEC model of a dielectric media cell is shown in Fig. 2. Here, C_1, C_2, V_L, I_{Ck1}, and I_{Ck2} are much the same as in Fig. 1. L_k represents the inductance of the bound current; resistor R_k represents the dielectric loss; and capacitor C_{ek} represents the excess capacitance effect in the interior of the cell [23].

After meshing the structure of the coreless PCB inductive components, analytic formulas can be used to calculate the partial inductance and partial coefficients of the potential (the inverse matrix of the short circuit capacitance) [15], [23]. As

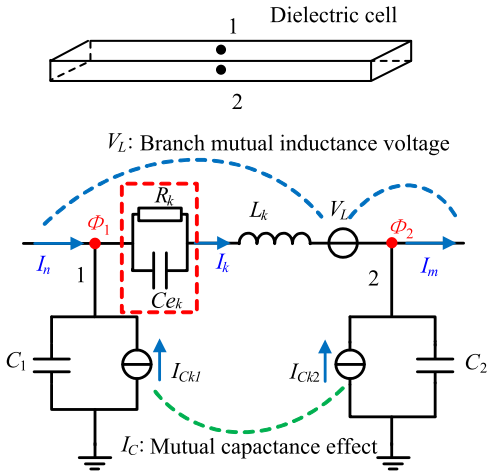

Fig. 2. Basic PEEC model of a dielectric cell.

PCB inductive components are planar in structure, both the conductors and dielectrics are thin in comparison to their length and width, so internal volume nodes can be ignored to simplify the meshing and calculations during the meshing and partial parameter calculation procedures. It should be noted that C_{ek} is in series with L_k in a dielectric PEEC model. This makes the relationship between the branch voltage and branch current complex and difficult to handle in the next MOR and parameter extraction procedures. Fortunately, the impedance of the series partial inductor L_k in a dielectric cell is much lower than the excess capacitor C_{ek} under the series self-resonance frequency of the branch, which is generally higher than ten gigahertz. So, L_k and V_L can be ignored, leaving just C_{ek} and R_k. For example, the self-resonance frequency of a typically sized FR4 material PCB dielectric cell that is $1 \times 1 \times 1$ mm, is about 24 GHz.

B. PEEC Matrix Formulation

By applying Kirchhoff's voltage law to the branch loop and Kirchhoff's current at each node, circuit equations can be formulated from the previous partial equivalent element models. Modified nodal analysis (MNA) is known to be an effective way of formulating matrices based on Kirchhoff's laws [24]. This is an easy approach to use for the analysis of electric circuits across the time and frequency domains. We therefore make use of MNA in our formulation of the PEEC circuit model as follows.

The general form given by MNA for a PEEC model is

$$\begin{bmatrix} \mathbf{G}+s\mathbf{C} & \mathbf{A}_L \\ \mathbf{A}_L^T & -(\mathbf{R}+s\mathbf{L}) \end{bmatrix} \begin{bmatrix} \mathbf{V}_n \\ \mathbf{I}_L \end{bmatrix} = \begin{bmatrix} \mathbf{I}_s \\ 0 \end{bmatrix} \tag{1}$$

where $\mathbf{A}_L$ is a node incidence matrix for the inductance branches; $\mathbf{C}$, $\mathbf{L}$, $\mathbf{R}$, and $\mathbf{G}$ are matrices for the capacitive, inductive, resistive, and conductive elements, respectively; $s = j\omega$ is the Laplace variable; $\mathbf{V}_n$ relates to the nodal voltages; $\mathbf{I}_L$ relates to the inductive branch currents; and $\mathbf{I}_s$ refers to the input currents for the network.

The inductive matrix $\mathbf{L}$ includes all self-inductance and mutual inductance aspects of the inductive branches and is a real symmetric matrix. The capacitive matrix $\mathbf{C}$ includes all self-capacitance and mutual capacitance aspects of conductor surface and dielectric cells. Furthermore, $\mathbf{C}$ can be also expressed by using

$$\mathbf{C} = \mathbf{A}_C \mathbf{C}_b \mathbf{A}_C^T \tag{2}$$

where $\mathbf{A}_C$ is a node incidence matrix for the capacitive branches. $\mathbf{C}_b$ is the branch capacitive matrix of the network and is a positive real diagonal matrix, because all capacitance values are physically positive. It is also worth noting that $\mathbf{A}_C \mathbf{C}_b \mathbf{A}_C^T$ can be proved to be a positive definite matrix because the branch capacitive matrix $\boldsymbol{C}_b$ is a positive real diagonal matrix.

From (1) earlier, the nodal admittance matrix $\mathbf{Y}_n$ of the PEEC network can be derived as follows:

$$\mathbf{Y}_n = \left(\mathbf{G} + s\mathbf{A}_C \mathbf{C}_b \mathbf{A}_C^T\right) + \mathbf{A}_L (\mathbf{R} + s\mathbf{L})^{-1} \mathbf{A}_L^T. \tag{3}$$

III. Physics-Based MOR and Parameter Extraction Methodology

There are two challenges to be faced during the procedures of MOR and key parameter quantization. The first is maintaining the consistency of the port impedance at the widest possible frequency range. The second is establishing the relationship between the circuit parameters determined by the physical structure and the port impedance. Fortunately, generalized eigenvalue theory is able to reveal the quantitative relationship among port impedance, branch inductance, nodal capacitance and its eigenvalues and eigenvectors [22]. The following sections therefore present the main principles of a physics-based MOR method based on generalized eigenvalue analysis.

A. Port Impedance Matrix Formulation

The port impedance matrix for the PEEC model can be derived by using electric network theory. The nodal voltages $\mathbf{V}_n$ equal the nodal impedance matrix $\mathbf{Z}_n$ multiplied by the excitation source matrix $\mathbf{I}_s$. This is shown as

$$\boldsymbol{V}_n = \boldsymbol{Z}_n \mathbf{I}_s = \mathbf{Y}_n^{-1} \mathbf{I}_s. \tag{4}$$

The port voltages $\mathbf{V}_{\text{port}}$ can be obtained from (4) by multiplying the node incidence matrix of the port, i.e., $\mathbf{B}_{\text{port}}^T$. At the same time, if the current sources matrix $\mathbf{I}_s$ is set to be the unit current excitation at the ports, that is $\mathbf{B}_{\text{port}}$, then the port impedance matrix $\mathbf{Z}_{\text{port}}$ can be derived as follows:

$$\boldsymbol{Z}_{\text{port}} = \mathbf{B}_{\text{port}}^T \mathbf{Y}_n^{-1} \boldsymbol{B}_{\text{port}}. \tag{5}$$

B. Physics-Based Model Reduction and Parameter Extraction

Prior research has established that the topology and branch parameters of an electric network determine its port characteristics, such as the port impedance, transfer functions, resonant frequency, and so on. On the other hand, for some specific electric networks, such as a lossless network, the parameters of branch inductance and nodal capacitance can be determined by the eigenfrequencies and eigenvectors of the network. This feature, which is based on generalized value theory from mathematics, is especially useful to set up an effective physical concise

lumped circuit model or extract inductance and capacitance parameters [25].

1) Generalized Eigenvalue Analysis for a Lossless Circuit: For a lossless PEEC network, both the **G** and **R** matrix are zero, so the nodal admittance matrix $\mathbf{Y}_n$ can be simplified from (3) as follows:

$$\mathbf{Y}_n = \frac{1}{s}\mathbf{A}_L\mathbf{L}^{-1}\mathbf{A}_L^T + s\mathbf{A}_C\mathbf{C}_b\mathbf{A}_C^T. \tag{6}$$

After transforming from the *S* domain into the frequency domain, the earlier equation can be rewritten as follows:

$$j\omega\mathbf{Y}_n = \mathbf{A}_L\mathbf{L}^{-1}\mathbf{A}_L^T - \omega^2\mathbf{A}_C\mathbf{C}_b\mathbf{A}_C^T. \tag{7}$$

It can be seen that $\mathbf{A}_L\mathbf{L}^{-1}\mathbf{A}_L^T$ and $\mathbf{A}_C\mathbf{C}_b\mathbf{A}_C^T$ are symmetric real matrices. Furthermore, $\mathbf{A}_C\mathbf{C}_b\mathbf{A}_C^T$ is a positive definite matrix as mentioned in the Section II-B. So, $j\omega\mathbf{Y}_n$ defines a generalized eigenvalue problem, enabling Theorem 3 in Appendix to be brought to bear. The nodal impedance matrix $\boldsymbol{Z}_n$ can now be derived and expressed according to A.2 in Appendix as follows:

$$\mathbf{Z}_n = \mathrm{j}\omega\sum_{k=1}^{K}\frac{1}{\omega_k^2-\omega^2}\mathbf{v}_k\mathbf{v}_k^T \tag{8}$$

where ω_k^2 is an eigenvalue, i.e., ω_k is an eigenfrequency or a resonant frequency; $\mathbf{v}_k$ is the eigenvector corresponding to ω_k^2; ω is the angle frequency; and *K* is the number of eigenvalues. Similarly, the port impedance matrix for this lossless network can be derived from (5) and (8) as follows:

$$\mathbf{Z}_{\mathrm{port}} = j\omega\sum_{k=1}^{K}\frac{1}{\omega_k^2-\omega^2}\left(\mathbf{B}_{\mathrm{port}}^T\mathbf{v}_k\right)\left(\mathbf{B}_{\mathrm{port}}^T\mathbf{v}_k\right)^T. \tag{9}$$

At the same time, the $\mathbf{A}_L\mathbf{L}^{-1}\mathbf{A}_L^T$ and $\mathbf{A}_C\mathbf{C}_b\mathbf{A}_C^T$ matrices can also be recovered according to A.3 in Appendix as follows:

$$\mathbf{A}_L\mathbf{L}^{-1}\mathbf{A}_L^T = \mathbf{X}^{-T}\wedge\mathbf{X}^{-1} \tag{10}$$

$$\mathbf{A}_C\mathbf{C}_b\mathbf{A}_C^T = \mathbf{X}^{-T}\mathbf{X}^{-1} \tag{11}$$

where $\mathbf{X}$ is the matrix whose columns are formed by the eigenvectors, $\mathbf{X} = (\mathbf{v}_1, \ldots, \mathbf{v}_K)$; and Λ is the diagonal matrix $\wedge = \mathrm{diag}\,(\omega_1^2, \omega_2^2 \ldots, \omega_K^2)$.

From (8) to (11), it can be seen that for a lossless network, the eigenvalues and eigenvectors of the matrix $j\omega\mathbf{Y}_n$ can determine not only the node impedance and port impedance of the network, but also the branch inductance and capacitance parameters when the network's topology is known. This provides an effective theoretical basis and method for the subsequent extraction of inductance and capacitance parameters from a complex network.

2) Model Reduction and Parameter Extraction Method: Considering the requirements on broadband and physically meaning, the MOR and parameter extraction from a PEEC network with a large number of partial inductors, capacitors, and resistors can be divided into two major parts. For inductance and capacitance parameters, the eigenvalue theory of the lossless network in the previous subsection can be used. For resistance parameters of the reduced order model, skin effect is considered to calculate or extract the resistance for the sake of simplicity.

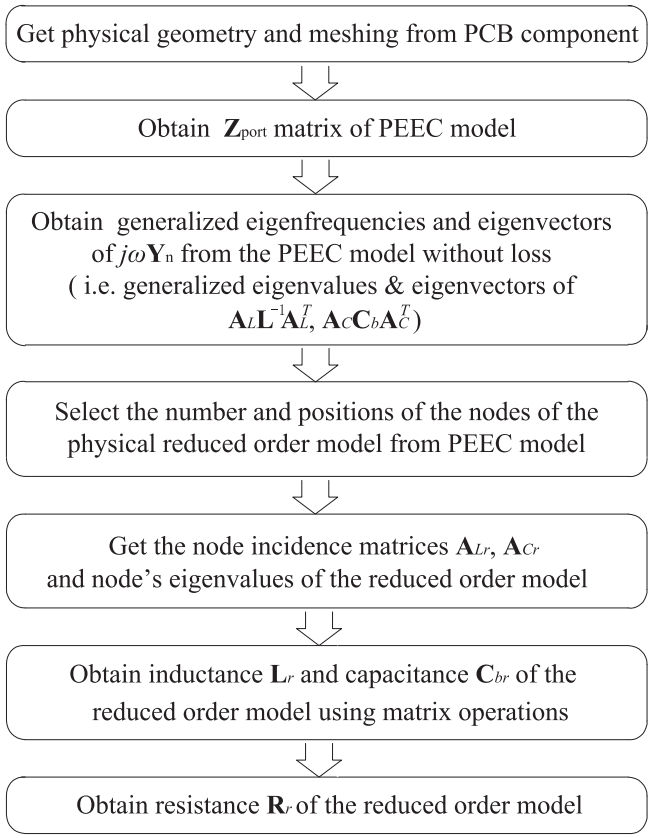

Fig. 3. Main steps of broadband pyhsical concise ciruit modeling method.

Then, the main steps required for the concise circuit model and parameter extraction method proposed in this article are outlined in Fig. 3.

A detailed PEEC model is first of all set up from the passive component's geometry. The model will contain enough number mesh cells to accurately describe the port impedance characteristics in as broad a frequency range as possible, such as 2 to 3 times the required frequency range. Then, the port impedance $\mathbf{Z}_{\mathrm{port}}$ matrix of the PEEC model can be calculated. After this, the eigenfrequencies and eigenvectors for the $j\omega\mathbf{Y}_n$ matrix are calculated and analyzed while all resistance is ignored and treated as zero. Taking into account the requirements for the frequency range and impedance accuracy, the number of nodes and positions of the reduced order model can be chosen. For example, if there are *N* eigenfrequencies that are lower than the highest frequency of interest (*N* is not more than *K* and generally far less than the order of $\mathbf{Y}_n$ matrix.), then at least $N+1$ nodes should be selected for the conductors in the PEEC model (nb. one of these nodes is selected as a potential reference point, so it does not appear in the MNA equations). The chosen nodes will subsequently be treated as new nodal in the reduced order model, with new node incidence matrices $\mathbf{A}_{Lr}$ and $\mathbf{A}_{Cr}$ then being established as well. The eigenvector values of these chosen nodes can be determined directly from their eigenvector values of the $j\omega\mathbf{Y}_n$ matrix of the lossless network too.

According to the generalized eigenvalue Theorem 3, as shown in (10) and (11), the relationship between the inductance

matrix $\mathbf{L}_r$, capacitance matrix $\mathbf{C}_{br}$ and the eigenfrequency and eigenvector still exists for the reduced order lossless model. So, the following equations can be applied:

$$\mathbf{A}_{Lr}\mathbf{L_r}^{-1}\mathbf{A}_{Lr}^{T} = \mathbf{X}_r^{-T} \wedge_{\boldsymbol{r}} \mathbf{X}_r^{-1} \tag{12}$$

$$\mathbf{A}_{Cr}\mathbf{C}_r\mathbf{A}_{Cr}^{T} = \mathbf{X}_r^{-T}\, \mathbf{X}_r^{-1} \tag{13}$$

where $\mathbf{A}_{Lr}$ and $\mathbf{A}_{Cr}$ are the inductance and capacitance node incidence matrices of the reduced order model, respectively; and $\mathbf{\Lambda}_r$ is a diagonal matrix, $\wedge_{\boldsymbol{r}} = \text{diag}\,(\omega_1^2,\, \omega_2^2 \ldots, \omega_N^2)$ and $\omega_1, \omega_2, \ldots < \omega_N$ is an eigenfrequency of the original PEEC model; $\mathbf{X}_r$ is the eigenvector value matrix for the chosen nodes at ω_1, ω_2, …and ω_N frequencies, thus:

$$\mathbf{X_r} = \mathbf{B}_n^T\, (\mathbf{v}_1, \ldots, \mathbf{v}_N) \tag{14}$$

where $\mathbf{B}_n^T$ is the node incidence matrix of the chosen nodes in the original PEEC model.

After this, the $\mathbf{L}_r$ matrix of the reduced order model can be obtained as follows, with $\mathbf{A}_{Lr}$ having an inverse matrix:

$$\mathbf{L}_r = \left[\mathbf{A}_{Lr}^{-1}\mathbf{X}_r^{-T} \wedge_r \mathbf{X}_r^{-1}\mathbf{A}_{Lr}^{-T}\right]^{-1}. \tag{15}$$

The $\mathbf{C}_{br}$ matrix of the reduced order model can be established as follows:

$$\mathbf{C}_{br} = \left[\mathbf{A}_{Cr}^T\mathbf{A}_{Cr}\right]^{-1}\left[\mathbf{A}_{Cr}^T\mathbf{X}_r^{-T}\mathbf{X}_r^{-1}\mathbf{A}_{Cr}\right]\left[\mathbf{A}_{Cr}^T\mathbf{A}_{Cr}\right]^{-1}. \tag{16}$$

After the inductance and capacitance parameters have been found as earlier, the loss aspects associated with the conductors will need to be considered in order to improve the accuracy of the reduced order model. However, the skin effect and proximity effect make the resistance of a PCB conductor not only frequency variable, but also difficult to express accurately with an analytical expression [26], [27]. Although 3-D discretization of the conductors with a maximum cell size of half the skin depth δ can be undertaken, this leads to a huge number of cells for the conductors, making the reduced order model meaningless. So, an empirical skin effect approximation formula shown in (17), is adapted to calculate the frequency variable resistance of the conductors for simple here, which ignores proximity and other high frequency effects [26], [27]. The $\mathbf{R_r}$ matrix of the MNA equation of the reduced order model can then be set up using these values to simplify the analysis and calculation

$$r\,(f) = \begin{cases} \rho\frac{l}{wt}\,, & 0 < f < \frac{\rho}{4\pi\mu_0(\min(w,t))^2} \\ \frac{\sqrt{\pi\mu_0\rho f}}{2(w+t)}\, l\, \Phi_{\text{Condrec}}\,, & f > \frac{\rho}{4\pi\mu_0(\min(w,t))^2} \end{cases} \tag{17}$$

where μ_0 is the permeability in a vacuum; ρ is the resistivity of the conductor; l is the length of the conductor, and t and w are the height and width of the rectangular cross-shaped conductor, respectively. Φ_{condrec} is correction factor for rectangular cross-shaped conductor and it contains the geometrical and frequency dependencies [27].

So far, the resistance, inductance and capacitance parameters of the reduced order model have been obtained. Similar to the MNA analysis in Section II-B, the port impedance $\mathbf{Z}_{\text{portr}}$ of the reduced order model can be calculated as

$$\boldsymbol{Z}_{\text{portr}} = \boldsymbol{B}_{\text{portr}}^T\left[s\boldsymbol{A}_{Cr}\boldsymbol{C}_{br}\boldsymbol{A}_{Cr}^T + \boldsymbol{A}_{Lr}(\boldsymbol{R}_r + s\boldsymbol{L}_r)^{-1}\boldsymbol{A}_{Lr}^T\right]^{-1}\boldsymbol{B}_{\text{portr}} \tag{18}$$

where $\mathbf{B}_{\text{portr}}$ is the unit current excitation at the ports of the reduced order model; $\mathbf{A}_{Lr}$ and $\mathbf{A}_{Cr}$ is the inductance and capacitance node incidence matrices of the reduced order model, respectively; and $\mathbf{L}_r$, $\mathbf{C}_{br}$ and $\boldsymbol{R}_r$ is the inductance, capacitance and resistance matrix of the reduced order model, respectively.

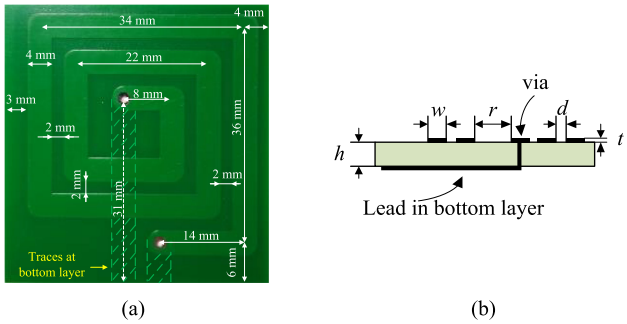

Fig. 4. Planar spiral inductor structure. (a) Top view. (b) side view.

IV. Planar Inductive Component Broadband Model

Two kinds of coreless planar inductive devices were designed and tested to verify the feasibility of the proposed concise physical circuit model and the parameter extraction method. The first was a two-layer spiral planar inductor. We will look at the concise modeling procedure for this inductor in detail. Then, a double-wound coreless planar transformer was modeled and analyzed in a similar fashion. All the modeling and calculation in this article are done using MATLAB 2014a software, and the calculation time is not more than 6 min on current commercial desktop computer.

A. Concise Broadband Planar Spiral Inductor Model

1) PEEC Model of Planar Coreless Spiral Inductor: Planar inductors are usually quadrate or circular spirals. The top and side view of the quadrate inductor we used here is shown in Fig. 4. The conductor material was copper. The width *w* of traces on the PCB was 4 mm, the height *t* was 0.035 mm and the line gap *d* was 2 mm. The thickness *h* of the board was 0.6 mm. The PCB material was FR4 and its relative permittivity was 4.2. The diameter *r* of the internal gap was 8 mm.

The PEEC modeling of this inductor included copper conductor modeling and FR4 dielectric modeling. The modeling of the conductors involved simplified meshing, which was then completed using the plane-structure of the PEEC cell because the height was thin. Fig. 5 shows the general mesh of the traces macroscopically. X_n represents the horizontal mesh and Y_n represents the vertical mesh. PIN_n represents the pin mesh. The red dots on the PINs are the external input nodes of the inductor. During meshing, the skin resistance, as per (17), was

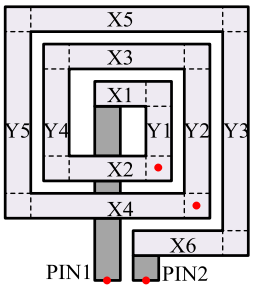

Fig. 5. Mesh layout for the traces.

used to simplify the cell size requirements and calculations. The dielectric material FR4 was meshed as excess capacitors at its surface nodes. This was described in Section II–A. Finally, the inductor was divided into a total of 697 inductive cells and 420 capacitive cells. This is a complex electric network and the order of the nodal admittance matrix $\mathbf{Y}_n$ was 419 after removing the infinity reference point.

The input impedance of the inductor was calculated by using (5). The predicted impedance magnitude-frequency curve is shown by the solid line in Fig. 6. The impedance of the inductor was measured by Agilent4294a and Agilent4396b impedance analyzer from 40 Hz to 1 MHz and from 1 MHz to 1.8 GHz respectively, the curves for which are also shown in Fig. 6. The predicted input impedance using the PEEC model closely matched the measured impedance up to 1.2 GHz (the yellow line). These results confirm the effectiveness of the PEEC model. Furthermore, there are several obvious resonant peaks between 40 Hz and 1.8 GHz, which are actually eigenfrequency.

2) MOR and Parameter Extraction: For this, the copper conductors in the PEEC model were set to be lossless. The generalized eigenvalues of the matrix $j\omega\mathbf{Y}_n$ of the lossless PEEC model were then solved using MATLAB R2014a software. The calculated eigenfrequencies included 265 MHz, 660 MHz, 1.09 GHz, and 1.41 GHz etc. These eigenfrequencies can also be found from the peak frequencies of the input impedance-frequency curve in Fig. 6(b). These peaks are caused by the parallel resonance of the PEEC network.

As electronic and EMC engineers are often concerned with the performance of inductors in a narrower band and want to use simple circuit models rather than complex PEEC models, it is useful to have a reduced order model with clear parameters. This article is focused on the frequency band from dc to 700 MHz. The 265 and 660 MHz eigenfrequencies fall within this band. For the sake of accuracy, the first three eigenfrequencies, 265 MHz, 660 MHz, and 1.09 GHz were selected as the eigenfrequencies in the reduced order model. The reduced order model should have at least one more node than the number of eigenfrequencies. Thus, there should be $3 + 1$ nodes. One of these nodes is the reference node. We, therefore, selected four nodes for the physical geometry. These are shown in Fig. 5 as red points. Two of them are the input pins of the inductor. The others are located at the corners of the internal loops.

Using (15) and (16), the reduced order model and its inductive and capacitive parameters were obtained. Fig. 7 shows the

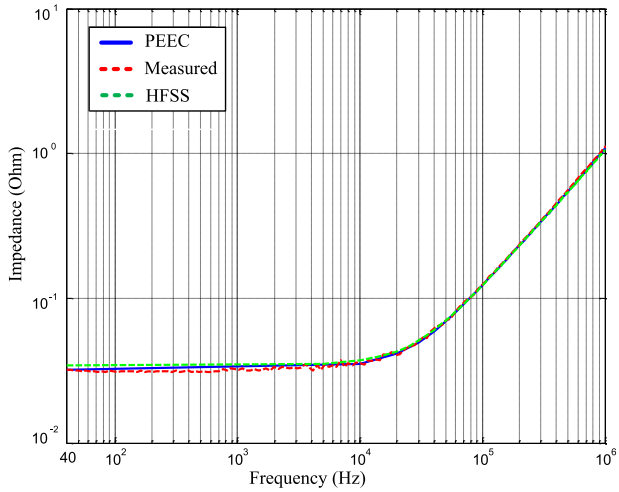

Fig. 6. Predicted and measured input impedance of the planar inductor. (a) 40 Hz–1 MHz. (b) 1 MHz–1.8 GHz.

TABLE I
REDUCED ORDER INDUCTOR MODEL PARAMETERS

Component	Value	Component	Value
L_1	38.2 nH	M_{12}	18.3 nH
L_2	24.3 nH	M_{13}	9.1 nH
L_3	28.1 nH	M_{23}	8.7 nH
C_1	1.46 pF	C_4	2.16 pF
C_2	0.37 pF	C_5	3.78 pF
C_3	0.17 pF	C_6	1.00 pF

inductive and capacitive circuit for the reduced order model and Table I lists the extracted inductance and capacitance parameters.

After the inductance and capacitance parameters of the reduced order model had been established, the modified skin resistance effect was used to correct the MNA of the reduced order model. Fig. 8 shows the predicted input impedance curve for the

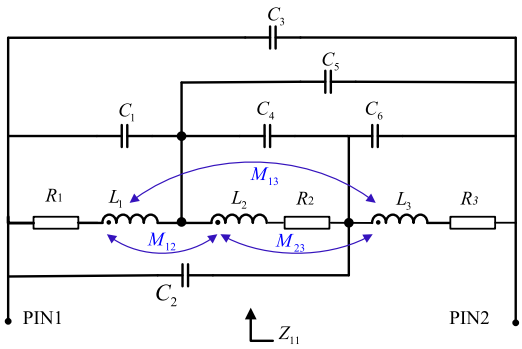

Fig. 7. Reduced order inductance and capacitance model of the inductor.

TABLE II
QUALITY FACTORS OF REDUCED ORDER INDUCTOR MODEL

Frequency	1 MHz	10 MHz	50 MHz	100 MHz	220 MHz
Measured Q	18.4	117.6	187.2	155.5	16.1
Calculated Q of MOR	23.9	178.3	220.2	189.5	23.2

four-node simplified model and the measured input impedance curve. It can be seen that the reduced order model is accurate up to 700 MHz, except that the resonance points are slightly higher. Table II shows the measured and calculated quality factors Q for the reduced order model. For Q value is very sensitive to the value of the resistance, the error of empirical formula (17) lead to some differences between the measured and calculated Q values, but the overall trend of them is the same. In addition, the Q calculated by the model is higher than the measured value, which results in under-damping phenomenon of the reduced order model during oscillation.

Note in particular that the number of parameters in the reduced order model is significantly less that it was in the orginal PEEC model. The original model had 243017 inductive and 87990 capacitive parameters. The reduced model had only six inductive parameters and six cap active parameters.

B. Concise Planar Coreless Transformer Model

1) PEEC Model of the Planar Coreless Transformer: The basic structure of a planar coreless transformer is also usually a quadrate spiral. The transformer has primary and secondary windings that are parallel in a vertical direction and it is built on a four-layer PCB. A top and side view is shown in Fig. 9. For this model, the primary winding was on the first and second layer, the secondary winding on the third and bottom layer. The ratio of primary turns to secondary turns was 4:4. The width w of the copper traces was 1 mm and the line gap d on the same layer was 1 mm. The height of the traces on the top and bottom layer was 0.035 mm, the height of the traces on the middle layer was 0.017 mm. The thickness of the second dielectric layer was 1.2 mm and the thickness of the other dielectric layers was 0.2 mm. The PCB material was FR4 with a relative permittivity of 4.2. The internal diameter r was 7 mm.

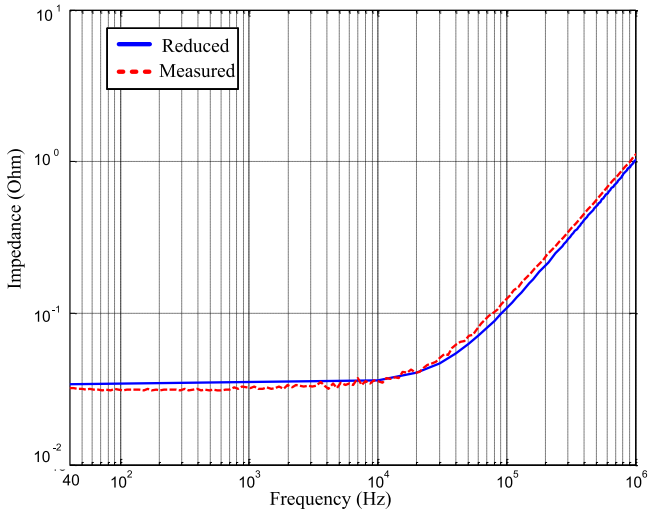

(a)

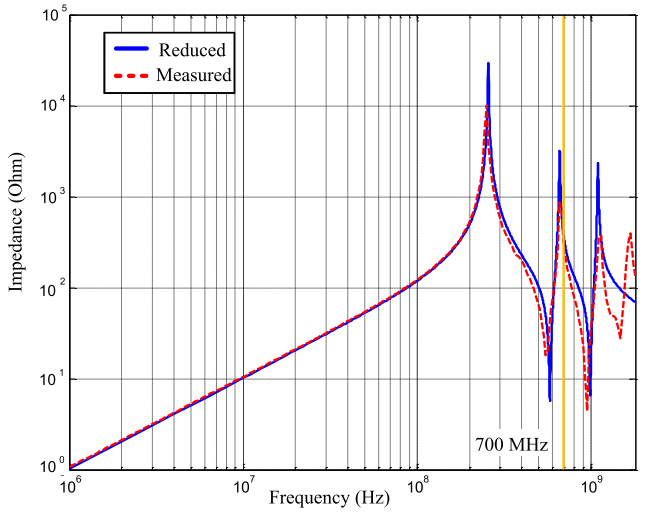

(b)

Fig. 8. Input impedance magnitude curves. (a) 40 Hz–1 MHz. (b) 1 MHz–1.8 GHz.

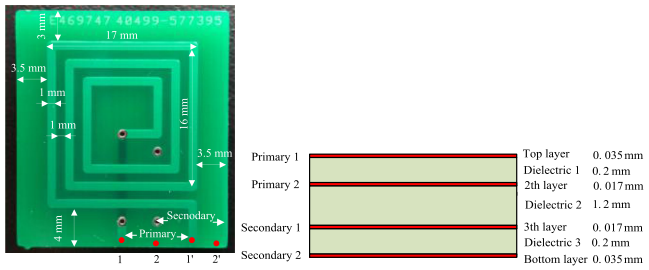

(a) (b)

Fig. 9. Planar transformer structure. (a) Top view. (b) Side view.

The PEEC modeling procedure for the transformer was similar to the PCB inductor above, so we will not go into further detail here. In the end, the transformer was divided into a total of 170 inductive cells and 172 capacitive cells.

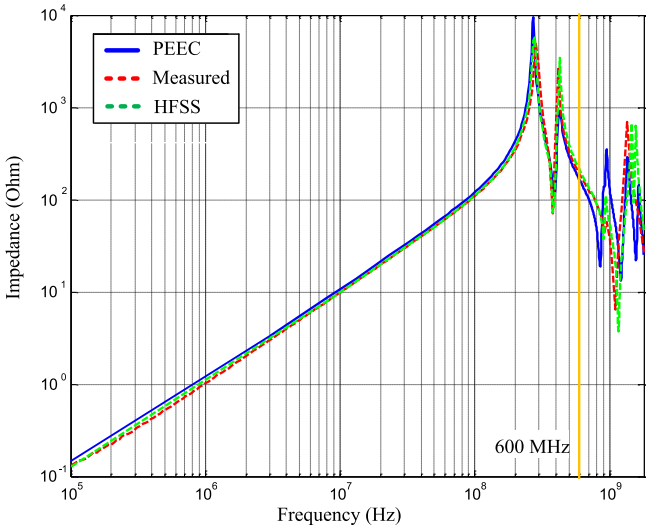

Fig. 10. Port impedance magnitude curves.

TABLE III
REDUCED ORDER TRANSFORMER MODEL PARAMETERS

Component	Value	Component	Value
C_1	0.13 pF	C_4	2.67 pF
C_2	0.105 pF	C_5	1.219 pF
C_3	2.514 pF	C_6	1.457 pF
L_1	160.0 nH	M_{12}	95.7 nH
L_2	152.2 nH	-	-

The port impedance of the transformer was predicted by the PEEC model and measured by the Agilent4396b impedance analyzer. The predicted and measured primary input impedance curves while the secondary input was open are shown in Fig. 10. There are several obvious peaks between 100 kHz and 1.8 GHz. The predicted and measured impedance were in fairly close agreement until 600 MHz. The port impedance for the secondary input produced similar results. These results confirm the effectiveness of the PEEC model.

2) MOR and Parameter Extraction: The generalized eigenvalues of the $j\omega\mathbf{Y}_n$ matrix for the lossless transformer PEEC model were calculated and included the following eigenfrequencies, which could also be found from the peak frequencies in Fig. 10: 270.2, 422.5, 911.3, and 951.6 MHz.

To get the reduced order model and its parameters we first of all designated the highest frequency of interest to be 500 MHz. The 270.2 and 422.5 MHz eigenfrequencies fall in this band. Four nodes were chosen and assigned to each of the four terminals of the transformer, as shown in Fig. 9(a). Following the steps outlined in Fig. 3, we obtained the physical concise transformer model and its inductive and capacitive parameters. Fig. 11 shows the inductive and capacitive circuits of the reduced order transformer model. Table III lists the extracted inductance and capacitance parameters. Note that the capacitive parameters were slightly asymmetric. This is because the primary and secondary input traces had an asymmetric structure.

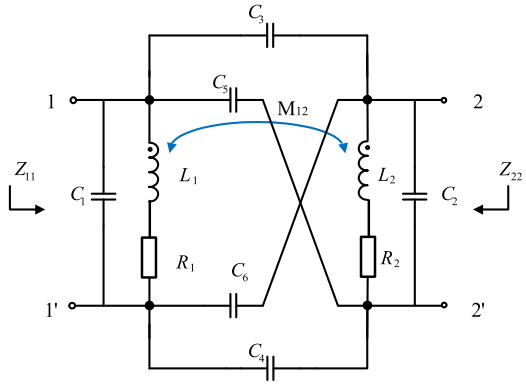

Fig. 11. Reduced order inductance and capacitance model of the transformer.

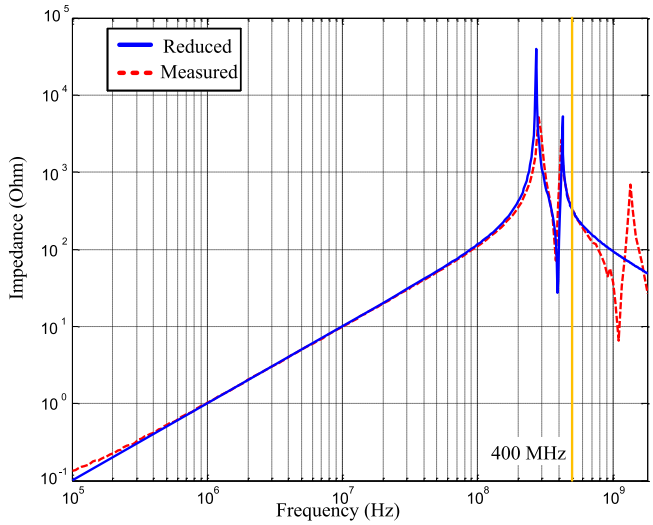

Fig. 12. Input impedance magnitude curves.

After the MNA of the reduced order model was corrected with the skin resistance, the predicted input impedance curve for the four-node concise model and the measured input impedance curve were plotted, as shown in Fig. 12. The curves are in fairly close agreement until 400 MHz, apart from some resonant frequency peaks. On the basis of the concise model, the Z_{12} primary and secondary impedance curves were also calculated and measured, as shown in Fig. 13. In addition, the primary to secondary transfer parameter S_{21} was simulated for the concise model and measured by an Agilent4396b network analyzer. The curves for this are shown in Fig. 14. The magnitudes and trends of both the impedance and *S*-parameter curves were well-matched in about 400 MHz range, confirming once again the validity of the model and the parameters. Table IV also shows the measured and calculated quality factors Q for primary of the reduced order model. It can be seen that there exist some differences between the measured and calculated Q values, but the overall trend of them is the same. Similarly, underdamping phenomenon of the reduced order model happens for higher Q.

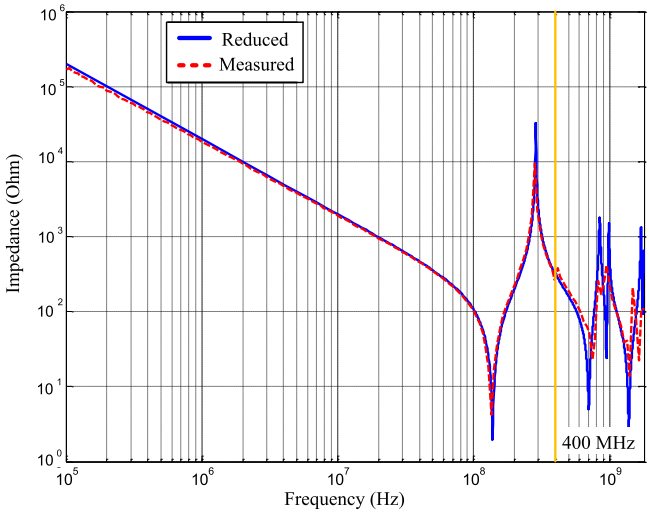

Fig. 13. Z_{12} primary and secondary impedance curves.

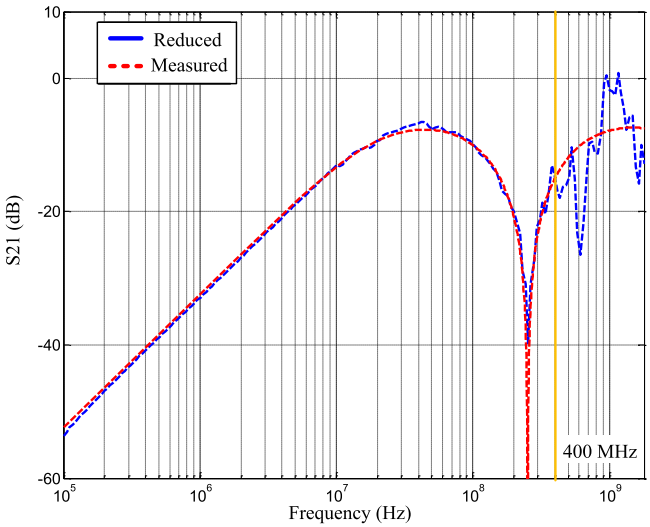

Fig. 14. Primary to secondary S_{21} curves.

TABLE IV
QUALITY FACTORS OF REDUCED ORDER TRANSFORMER MODEL

Frequency	1 MHz	10 MHz	50 MHz	100 MHz	220 MHz
Measured Q	7.4	45.7	93.6	103.7	29.4
Calculated Q for MOR	5.8	47.8	113.0	112.7	44.2

C. Errors and Node Selection

Inevitably, the reduced order model does produce some errors and sometimes the extracted parameters are also abnormal. In this section, we discuss the possible reasons and countermeasures.

A consequence of removing the higher eigenfrequencies to get the reduced order model is that the $\mathbf{Z}_{\mathrm{portr}}(\omega)$ in the reduced order model differs from the $\mathbf{Z}_{\mathrm{port}}(\omega)$ in the original PEEC model. This error mainly relates to the removed terms. For example, the error $\Delta(\omega)$ in the four-node reduced order model of the planar PCB inductor can be expressed as in (18), because only the first three eigenfrequencies of the inductor were chosen in the reduced order model. According to this equation, as many eigenvalues as possible should be chosen, unless the complexity of the reduced order model becomes unacceptable

$$\Delta(\omega) = \sum_{k=4}^{K419} \frac{j\omega}{\omega_k^2 - \omega^2} (\mathbf{B}_{\mathrm{port}}^T \mathbf{v}_k)(\mathbf{B}_{\mathrm{port}}^T \mathbf{v}_k)^T. \tag{19}$$

It can also be seen that the coefficient for each item in the previous equation is as follows:

$$\mathrm{coef} = \frac{j\omega}{\omega_k^2 - \omega^2}. \tag{20}$$

This coefficient can be understood as weight. The greater the extent to which the chosen frequency is less than the unselected eigenfrequencies, the less the weight of the coef and the smaller the error.

During the parameter extraction procedures, we have discussed, it was found that a negative capacitance value can sometimes occur when certain node positions are chosen. This is abnormal because all capacitance should be positive. It is possible that nonprojectional meshing may be present for some geometry, resulting in a negative capacitance in the model. Another possible reason is the Δ error, covered by (18). Our own experience also suggests that negative capacitance can happen if two nodes are too close to one another. This being so, ensuring there is an even distance between the nodes should reduce the likelihood of this issue arising.

Similarly, the resistance formula in the simplified model produces high-frequency errors due to neglecting the proximity effect and the rectangular corner influence. A more accurate estimation formula can make the resonance prediction better. More thorough investigation of the various problems we encountered and the development of better countermeasures will be the next step in our research.

V. CONCLUSION

This article has proposed a novel approach to concise broadband physical circuit modeling and parameter extraction, based on PEEC and generalized eigenvalue theory. It is particularly effective for the functional design of high frequency circuits and EMC predictions. It offers the following contributions.

1) Demonstration of the viability of establishing a precise PEEC model and MNA equation under quasi-static electromagnetic field conditions by preserving excess capacitance only in the dielectric volume cell. This makes the node admittance matrix easier to deal with in later analysis and calculation.
2) A novel broadband physical circuit modeling and MOR methodology that uses generalized eigenvalue theory and PEEC theory. Detailed theoretical formulations and key

MOR steps were provided and its effectiveness was verified by testing its use for the modeling of two planar PCB inductive components.

3) Analysis of the key issues, such as the position and number of nodes selected, negative capacitance, and the skin resistance effect and the proposal of countermeasures to improve the accuracy of the reduced order model.

There is still some work to be done in the near future to achieve better practicality, such as automating selection of the optimum positions for the nodes, PEEC modeling of magnetic materials, etc.

APPENDIX
GENERALIZED EIGENVALUE THEORY

The definition of a generalized linear eigenvalue is as follows [22], [25]:

$$[\mathbf{A} - \lambda\mathbf{B}]\,\mathbf{x} = 0 \tag{A.1}$$

where $\mathbf{A}$ and $\mathbf{B}$ are square matrices, $\mathbf{x}$ is a vector, and λ is a number. If a non-trivial ($\mathbf{x}$, λ) exists and it satisfies (A.1), ($\mathbf{x}$, λ) is defined as an eigenpair. The set of all eigenpairs forms the spectrum $\{(\mathbf{x}_\mathrm{k},\ \lambda_\mathrm{k}),\ \mathrm{k} \in \mathbf{K}\}$.

Theorem 1: For a real and symmetric $\mathbf{A}$ and $\mathbf{B}$, the eigenpairs ($\mathbf{x}_k$, λ_k) are real and can be chosen to satisfy the orthogonal relation $\mathbf{x}_k^T\mathbf{B}\mathbf{x}_l = 0, k \# l$.

Theorem 2: For a real and symmetric $\mathbf{A}$ and $\mathbf{B}$, where $\mathbf{B}$ is definitely positive, there exists a complete set of real eigenpairs $\{(\mathrm{x_k},\ \lambda_\mathrm{k}),\ \mathrm{k} = 1, \ldots,\ \mathrm{K}\}$ with $\mathbf{x}_k^T\mathbf{B}\mathbf{x}_l = \delta_{kl}$. δ_{kl} being the Kronecker Delta.

Theorem 3: For a real and symmetric $\mathbf{A}$ and $\mathbf{B}$, if $\mathbf{B}$ is definitely positive, then

$$[\mathbf{A} - \lambda\mathbf{B}]^{-1} = \sum_{k=1}^{K} \frac{1}{\lambda_k - \lambda}\mathbf{x}_k\mathbf{x}_k^T. \tag{A.2}$$

If we set $\mathbf{X}$ as the matrix whose columns are formed by the eigenvectors $\mathbf{X} = (\mathbf{x}_1, \ldots, \mathbf{x}_K)$, $\mathbf{A}$ and $\mathbf{B}$ can be recovered from the eigenvectors $\mathrm{x_k}$ by solving the linear system of equations

$$\mathbf{X}^T\mathbf{A}\mathbf{X} = \begin{pmatrix} \lambda_1 & \cdots & 0 \\ \vdots & \ddots & \vdots \\ 0 & \cdots & \lambda_K \end{pmatrix} \quad \mathbf{X}^T\mathbf{B}\mathbf{X} = \mathbf{E} \tag{A.3}$$

where the matrix $\mathbf{E}$ is an identity array of $K \times K$.

REFERENCES

[1] Y. Y. Lim, Y. M. Goh, M. Yoshida, T. T. Bui, M. Aoyagi, and C. Liu, "30-GHz high-frequency application of screen printed interconnects on an organic substrate," *IEEE Trans. Compon., Packag. Manuf. Technol.*, vol. 7, no. 9, pp. 1506–1515, Sep. 2017.

[2] N. Fichtenbaum, M. Giandalia, S. Sharma, and J. Zhang, "Half-bridge GaN power ICs: Performance and application," *IEEE Power Electron. Mag.*, vol. 4, no. 3, pp. 33–40, Sep. 2017.

[3] S. Wang, F. C. Lee, D. Y. Chen, and W. G. Odendaal, "Effects of parasitic parameters on EMI filter performance," *IEEE Trans. Power Electron.*, vol. 19, no. 3, pp. 869–877, May 2004.

[4] M. Laour, R. Tahmi, and C. Vollaire, "Modeling and analysis of conducted and radiated emissions due to common mode current of a Buck converter," *IEEE Trans. Electromagn. Compat.*, vol. 59, no. 4, pp. 1260–1267, Aug. 2017.

[5] C. Guo and T. H. Hubing, "Circuit models for power bus structures on printed circuit boards using a hybrid FEM-SPICE method," *IEEE Trans. Adv. Packag.*, vol. 29. no. 3, pp. 441–447, Aug. 2006.

[6] J. A. Martinez and B. A. Mork, "Transformer modeling for low- and mid-frequency transients—A review," *IEEE Trans. Power Del.*, vol. 20, no. 2, pp. 1625–1632, Apr. 2005.

[7] I. Stevanovic, S. Skibin, M. Masti, and M. Laitinen, "Behavioral modeling of chokes for EMI simulations," *IEEE Trans. Power Electron.*, vol. 28, no. 2, pp. 695–704, Feb. 2013.

[8] H. Lu, J. Zhu, and S. Y. R. Hui, "Experimental determination of stray capacitances in high frequency transformers," *IEEE Trans. Power Electron.*, vol. 18, no. 5, pp. 1105–1112, Sep. 2003.

[9] S. Raju, R. Wu, and M. Chan, "Modeling of mutual coupling between planar inductors in wireless power applications," *IEEE Trans. Power Electron.*, vol. 29, no. 1, pp. 481–490, Jan. 2014.

[10] Q. Zhang *et al.*, "Application of an improved multi-conductor transmission line model in power transformer," *IEEE Trans. Magn.*, vol. 49, no. 5, pp. 2029–2032, May 2013.

[11] I. F. Kovačević, T. Friedli, A. M. Muesing, and J. W. Kolar, "3-D electromagnetic modeling of EMI input filters," *IEEE Trans. Ind. Electron.*, vol. 61, no. 1, pp. 231–242, Jan. 2014.

[12] J. D. Owens and P. L. Chapman, "Automatic generation of accurate low-order models for magnetic devices," *IEEE Trans. Power Electron.*, vol. 20, no. 4, pp. 732–742, Jul. 2014.

[13] L. V. Ene *et al.*, "Simulation of magnetically coupled coils in Ansoft Q3D extractor program," in *Proc. 2017 Int. Conf. Optim. Elect. Electron. Equip., 2017 Int. Aegean Conf. Elect. Mach. Power Electron.*, Brasov, Romania, 2017, pp. 202–207.

[14] K. Jackman and C. J. Fourie, "Fast multicore FastHenry and a tetrahedral modeling method for inductance extraction of complex 3D geometries," in *Proc. 15th Int. Supercond. Electron. Conf.*, Nagoya, Japan, 2015, pp. 1–3.

[15] A. E. Ruehli, "Equivalent circuit models for three-dimensional multiconductor systems," *IEEE Trans. Microw. Theory Techn.* vol. 22, no. 3, pp. 216–221, Jul. 1974.

[16] M. Enohnyaket and J. Ekm An, "Analysis of air-core reactors from DC to very high frequencies using PEEC models," *IEEE Trans. Power Del.*, vol. 24, no. 2, pp. 719–729, Apr. 2009.

[17] M. A. Bazaz, M.-U. Nabi, and S. Janardhanan, "A review of parametric model order reduction techniques," in *Proc. 2012 IEEE Int. Conf. Signal Process., Comput. Control*, 2012, pp. 1–6.

[18] M. Rewienski and J. White, "A trajectory piecewise-linear approach to model order reduction and fast simulation of nonlinear circuits and micromachined devices," *IEEE Trans. Comput.-Aided Des. Integr. Circuits Syst.*, vol. 22, no. 2, pp. 155–170, Feb. 2003.

[19] N. Bondarenko *et al.*, "Development of simple physics-based circuit macromodel from PEEC," *IEEE Trans. Electromagn. Compat.*, vol. 58, no. 5, pp. 1485–1493, May 2016.

[20] Y. Dou and K. Wu, "A passive PEEC-based micromodeling circuit for high-speed interconnection problems," *IEEE Trans. Microw. Theory Techn.*, vol. 66, no. 3, pp. 1201–1214, Mar. 2018.

[21] F. Traub *et al.*, "Generation of physical equivalent circuits using 3D simulations," in *Proc. Int. Supercond. Electron. Conf.*, 2012, pp. 486–491.

[22] F. Traub *et al.*, "Eigenmodes of electrical components and their relation to equivalent electrical circuits," in *Proc. Int. Supercond. Electron. Conf.*, 2013, pp. 287–293.

[23] A. E. Ruehli and H. Heeb, "Circuit models for three-dimensional geometrices indlucing dielectrics," *IEEE Trans. Microw. Theory Techn.*, vol. 40, no. 7, pp. 1507–1516, Jul. 1992

[24] A. Brambilla, A. Premoli, and G. Storti-Gajani, "Recasting modified nodal analysis to improve reliability in numerical circuit Simulation," *IEEE Trans. Circuits Syst. I*, vol. 52, no. 3, pp. 522–534, Mar. 2005.

[25] Z. Bai *et al.*, "*A brief Tour of Eigenproblems, in Templates for the Solution of Algebraic Eigenvalue Problems*," Philadephia, PA, USA: SIAM, 1987, pp. 7–43.

[26] E. Bogatin, *Signal Integrity: Simplified*. Upper Saddle River, NJ, USA: Pearson Educ. Inc., 2004, pp. 338–356.

[27] I. Lope, C. Carretero, J. Acero, R. Alonso, and J. M. Burdio, "AC power losses model for planar windings with rectangular cross-sectional conductors," *IEEE Trans. Power Electron.*, vol. 29, no. 1, pp. 23–28, Jan. 2014.

Junping He (Member IEEE) received the bachelor's and master's degrees from the Northern Jiaotong University, Beijing, China in 1993 and 1999, and the Ph.D. degree from Tsinghua University, Beijing, China, in 2003, all in electrical engineering.

He was a Postdoctoral with Tsinghua University and Delta Power electronics center, Shanghai, China, from 2003 to 2005. In 2005, he joined the Harbin Institute of Technology, Shenzhen, China, where he is currently an Associate Professor. From 2013 to 2014, he was a Visiting Scholar in electromagnetic compatibility Laboratory, Missouri University of Science and Technology, Rolla, MO, USA. His research interests include electromagnetic compatibility analysis and design in power electronics, and renewable energy power generation.

Sili Tao received the bachelor's degree from the Harbin Institute of Technology, Harbin, China in 2014, and the master's degree from the Harbin Institute of Technology, Shenzhen, China, in 2018, respectively, both in electrical engineering.

Since 2018, he has been an Electrical Design Engineer with Hangzhou EV-Tech Co., Ltd., Hangzhou, China. He is mainly engaged in the development of the board charger and dc/dc converter for electric vehicle.

Huazhao Wu received the bachelor's degree from the Harbin Institute of Technology, Harbin, China, in 2012, and the master's degree from the Harbin Institute of Technology, Shenzhen, Shenzhen City, China, in 2019 respectively, both in electrical engineering.

He is currently a Technical Director of informatization section of Guigang industry and Information Bureau, Guigang, China.